Solar Phys
DOI 10.1007/s11207-012-0060-3

Nitrate in Polar Ice: A New Tracer of Solar Variability

R. Traversi · I.G. Usoskin · S.K. Solanki · S. Becagli · M. Frezzotti · M. Severi · B. Stenni · R. Udisti

Received: 23 April 2012 / Accepted: 18 June 2012

Abstract Knowledge of the long-term variability of solar activity is of both astrophysical and geoscientific interest. Reconstructions of solar activity over multiple millennia are traditionally based on cosmogenic isotopes ^{14}C or ^{10}Be measured in natural terrestrial archives, but the two isotopes exhibit significant differences on millennial time scales, so that our knowledge of solar activity at this time scale remains somewhat uncertain. Here we present a new potential proxy of solar activity on the centennial-millennial time scale, based on a chemical tracer, viz. nitrate content in an ice core drilled at Talos Dome (Antarctica). We argue that this location is optimal for preserving the solar signal in the nitrate content during the Holocene. By using the firn core from the same location we show that the 11-year and Gleissberg cycles are present with the variability of 10 – 25 % in nitrate content in the pre-industrial epoch. This is consistent with the results of independent efforts of modeling HNO_3 and NO_y in Antarctic near surface air. However, meteorological noise on the interannual scale makes it impossible to resolve individual solar cycles. Based on different

R. Traversi · S. Becagli · M. Severi · R. Udisti
Department of Chemistry "Ugo Schiff", University of Florence, Sesto F.no, 50019 Florence, Italy

I.G. Usoskin (✉)
Sodankylä Geophysical Observatory (Oulu Unit), University of Oulu, 90014 Oulu, Finland
e-mail: Ilya.Usoskin@oulu.fi

I.G. Usoskin
Department of Physics, University of Oulu, 90014 Oulu, Finland

S.K. Solanki
Max Planck Institute for Solar System Research, 37191 Katlenburg-Lindau, Germany

S.K. Solanki
School of Space Research, Kyung Hee University, Yongin, Gyeonggi 446-701, Republic of Korea

M. Frezzotti
ENEA, CR Casaccia, 00123 Roma, Italy

B. Stenni
Department of Mathematics and Geosciences, University of Trieste, 34127 Trieste, Italy

Published online: 19 July 2012

processes of formation and transport compared to cosmogenic isotopes, it provides new, independent insight into long-term solar activity and helps resolve the uncertainties related to cosmogenic isotopes as diagnostics of solar activity.

Keywords Cosmic rays, galactic · Holocene · Ice core · Nitrate · Solar cycle

1. Introduction

The Sun's activity varies between deep grand minima, such as the Maunder minimum when practically no sunspots were visible for several decades, to grand maxima of activity, such as the one in the second half of the 20th century (Eddy, 1976; Solanki *et al.*, 2004). A direct record of solar activity, in the form of sunspot numbers, exists since 1610, but knowledge of solar variability on even longer time scales is important for both astrophysics, since it sets important constraints on the physics of solar/stellar magnetic dynamos (Charbonneau, 2010; Nandy, Muñoz-Jaramillo, and Martens, 2011), and geosciences, since it allows improved assessments of the possible solar impact upon Earth (de Jager, 2005; Gray *et al.*, 2010). Solar activity is traditionally studied throughout the Holocene by using proxies based on cosmogenic radionuclides (^{10}Be and ^{14}C), produced by nuclear interactions of galactic cosmic rays (GCRs) with nuclei of atmospheric gases. Since the GCR flux near Earth is modulated by solar magnetic activity, the production rate of cosmogenic nuclides is inversely related to it (*e.g.*, Beer *et al.*, 1990; Solanki *et al.*, 2004; Stuiver and Braziunas, 1989). After production, the nuclides are stored in independently datable natural archives such as trees or polar ice (*e.g.*, Dorman, 2004). Terrestrial fates of the two isotopes are almost independent of each other, including different sensitivity to geomagnetic changes (Snowball and Muscheler, 2007; Usoskin *et al.*, 2006b) and regional/global climate changes (*e.g.*, Steig *et al.*, 1996; Oppo, McManus, and Cullen, 2003). Therefore, similarities in the temporal behavior of the ^{10}Be and ^{14}C records can be ascribed to the common signal of production, viz. solar activity (Bard *et al.*, 1997) while sources of discrepancy cannot be pin-pointed beyond their terrestrial origin. The two records are in very good agreement at time scales between $\approx$100 and 1000 years, but disagree at shorter (decades) and longer (millennia) time scales (Usoskin *et al.*, 2009; Vonmoos, Beer, and Muscheler, 2006). It is generally thought that the ^{10}Be signal can be distorted by the polar regional circulation at the multi-decadal time scale (Steig *et al.*, 1996; Stuiver and Braziunas, 1989; Lal, 2007), while ^{14}C can be affected, at millennial time scales, by the carbon cycle change during/after deglaciation (Oppo, McManus, and Cullen, 2003). However, so far the effect of these processes remain speculative, as does consequently, the true history of solar variability over millennia. Therefore, any independent information on past solar activity variations is extremely valuable.

Here we report on a novel long-term proxy of solar activity using nitrate records from an Antarctic ice core recently drilled at Talos Dome (East Antarctica) in the framework of the TALDICE Project.

In addition to terrestrial sources, limited to the troposphere, nitrate (NO_3^-) concentration in polar regions has relevant stratospheric sources (Legrand and Kirchner, 1990; Savarino *et al.*, 2007), related to extraterrestrial fluxes of energetic particles and solar irradiation. It is sometimes speculated that large solar energetic particle (SEP) events can lead to distinguishable nitrate spikes in high-resolution stratigraphies from polar ice cores (Zeller and Parker, 1981; Shea *et al.*, 2006; Kepko *et al.*, 2009). This, however, requires either very fast and focused polar precipitation of nitrate from the stratosphere that is unlikely and can be masked by local meteorological or anthropogenic events (Wolff *et al.*, 2008, 2012), or an essentially

tropospheric production which is not reproduced by models (Egorova *et al.*, 2011). However, our results are not related to those studies and suggest that SEP events do not play a major role in the long-term nitrate variability. We note that a good agreement between the nitrate and ^{10}Be concentrations has been found recently at time scales longer than the solar cycle for the last 450 years, in a shallow Antarctic ice core IND-22/B4 in Dronning Maud Land (Laluraj *et al.*, 2010), suggesting a potential link between nitrate and solar activity on the centennial time scale. Although a number of nitrate ice core records covering the last glacial cycles is available (*e.g.*, Legrand and Mayewski, 1997; Röthlisberger *et al.*, 2000; Traversi *et al.*, 2002), earlier attempts to establish a stable relationship between nitrate content in polar ice and solar activity did not yield a consistent view, possibly due to additional nitrate sources (*e.g.*, Legrand and Kirchner, 1990). The latter include long-range transport from mid-latitudes (where it is produced by lighting), continental and marine input and emissions from snowpack (Grannas *et al.*, 2007). Alteration of nitrate records by post-depositional effects may also play a role (Grannas *et al.*, 2007; Honrath *et al.*, 1999; Wagnon, Delmas, and Legrand, 1999). However, high-resolution chemical and isotopical measurements performed on a firn core previously drilled at the Talos Dome site (TD96, 89 m deep firn core) showed the potential for achieving reliable geochemical and palaeoclimatic records from this site (Becagli *et al.*, 2004; Stenni *et al.*, 2002; Traversi *et al.*, 2004).

2. Data and Uncertainties

2.1. Data Records

Here we consider nitrate measurements performed along the TALDICE ice core (East Antarctica, 72°49′ S, 159°11′ E, 2315 m a.s.l.) reaching back to about 11 400 years before present (BP henceforth). The TALDICE ice core was processed during several sessions from 2006 to 2008 at the Alfred Wegener Institute in Bremerhaven (Germany). Firn strips (belonging to the 6 – 73 m depth range) were decontaminated by manual scraping in the cold room of the University of Florence and cut into discrete, 3.5 cm long samples. Ice sections (73 – 1620 m depth), typically 3.4 × 3.4 cm, were melted onto a hotplate and the liquid flow from the inner part of the core was distributed to various detectors (Continuous Flow Analysis and Fast Ion Chromatography systems) and collected in vials for later determination of main and trace ions by Ion Chromatography (Wolff *et al.*, 2010). Two different resolutions were chosen for the discrete sample collection: low resolution obtained by melting a whole 1-m long strip (bag mean) and collecting it in a single vial, and high resolution (about 7 cm). As the high-resolution analysis is currently in progress, we present here only the firn and bag mean data, both obtained at the University of Florence.

The ice samples covering the Holocene (645 – 11 400 years BP, 73 – 660 m depth) were dated using the TALDICE official timescale (TALDICE-1, see Buiron *et al.* (2011)). The bag means correspond to about 12 years at present time and about 30 years at the beginning of Holocene. In the considered temporal period, the dating uncertainty of the TALDICE core fluctuates between about 200 and 450 years showing values higher than 300 year in most of the Holocene (see the supplementary material of Schüpbach *et al.* (2011)). For further analysis these data have been averaged over 50-yr (yr = year) intervals as shown in Figures 1A and 1B. Firn samples have a sub-annual resolution (ranging between 0.2 and 0.3 years) and they were dated by transferring the latest dating of EPICA Dome C to the TALDICE ice core via volcanic signatures matching (Severi *et al.*, 2012) due to the high relative uncertainty of TALDICE-1 in the last millennium. The dating uncertainty during

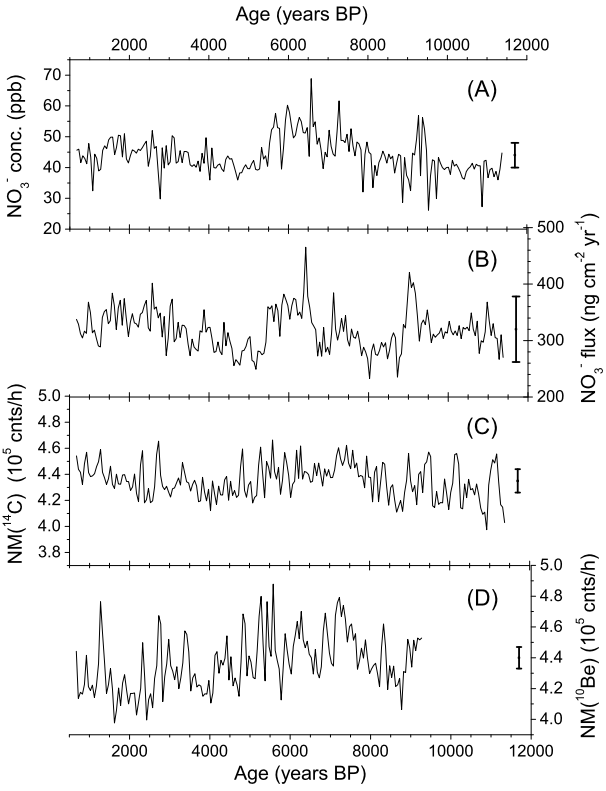

Figure 1 Long-term data used in this study (see text for definitions). All data sets are 50-yr averaged. Vertical bars on the right depict the uncertainties of the time series over the Holocene. Panels A and B refer to the concentration and flux, respectively, of nitrate measured in TALDICE ice samples spanning the Holocene (73 – 600 m depth, 1 m resolution). Panels C and D depict cosmic ray intensity (quantified in count rates of a standard polar neutron monitor) reconstructed from ^{14}C and ^{10}Be cosmogenic isotope records, respectively.

the last centuries is 2 – 5 years. The data have been annually averaged for further analysis, as shown in Figure 2A.

Because of the dominant dry deposition at Talos Dome (see Section 2.2 and Figure 3), nitrate flux NO_3(F) is supposed to be most representative of the nitrate content in the atmosphere. The nitrate flux NO_3(F) is not measured but calculated from the directly measured nitrate concentration NO_3(C) and the independently evaluated snow accumulation rate, whose significant uncertainties lead to nearly double the error in NO_3(F) compared to that of NO_3(C) (see Section 2.2). Since the accumulation rate is indistinguishable from a constant over the Holocene within the dating uncertainties (see Section 2.2 and Figure 4C), nitrate flux and concentration depict similar variability. Therefore, here we consider both the direct index NO_3(C) and the computed NO_3(F), shown in Figure 4A as standardized data series. As an index of solar variability we use the flux of GCR near Earth represented, following common practice, by the count rate of a hypothetical standard sea-level polar neutron monitor (McCracken and Beer, 2007; Usoskin *et al.*, 2002), which is insensitive to geomagnetic field changes. The count rate is computed using the heliospheric modulation potential and the neutron monitor yield function (Usoskin *et al.*, 2005). The modulation potential was reconstructed for the Holocene (Solanki *et al.*, 2004; Usoskin, Solanki, and Kovaltsov, 2007) from radiocarbon INTCAL ^{14}C data (Stuiver *et al.*, 1998; Reimer *et al.*, 2004), as well as from ^{10}Be data in the Greenland GRIP ice core (Finkel and Nishiizumi, 1997; Yiou *et al.*, 1997) for the last 9500 years (Steinhilber, Abreu, and Beer, 2008). The corresponding GCR fluxes are henceforth called CR(^{14}C) and CR(^{10}Be), respectively, and shown in Figures 1C and 1D, respectively. Uncertainties of CR(^{14}C) due to all known sources (Solanki

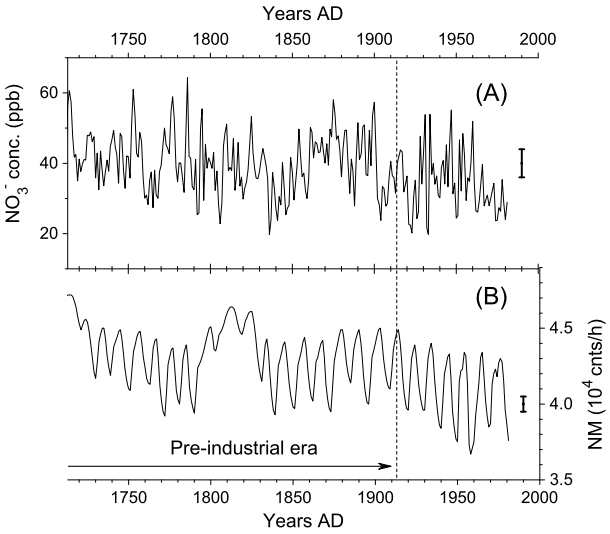

Figure 2 Data for the last centuries used in this study. All data sets are annually averaged. Vertical bars on the right depict the uncertainties of the time series. Panel A displays the nitrate concentration data from TALDICE firn samples covering the last 640 years (6 – 73 m depth, 3.5 cm resolution). Panel B depicts reconstruction of cosmic ray intensity from sunspot numbers after the Maunder minimum (actually measured intensities are used after 1951). The pre-industrial epoch is left of the vertical dashed line.

et al., 2004; Vieira *et al.*, 2011) are about 2 %. Uncertainties of CR(^{10}Be) are 1.5 % which correspond to 10 % in the heliospheric modulation potential as given by Steinhilber, Abreu, and Beer (2008), not including uncertainties in the geomagnetic field over the Holocene.

For further analysis, all data sets have been standardized, viz. the mean level removed and the residual divided by the standard deviation, as shown in Figure 4. For the shorter time interval of the last centuries, we make use of the annually averaged TALDICE firn data (Figure 2A) and CR flux as reconstructed from sunspot data, similarly to Usoskin *et al.* (2002), but using a recent solar open flux model (Krivova, Balmaceda, and Solanki, 2007; Vieira *et al.*, 2011). After 1951, the real CR data are used. This data series is plotted in Figure 2B.

2.2. Nitrate Depositional Processes at Talos Dome: Dry *vs.* Wet Deposition

Nitrate is deposited from the atmosphere to snow through wet and dry deposition. Dry deposition implies that the amount of the deposited specie is like sedimentation not affected by the variations in precipitation (snow accumulation rate). In such conditions, the deposited nitrate flux is a direct index of the nitrate concentration in near-ground air. On the contrary, wet deposition implies removal of nitrate from air by snow precipitation, and, accordingly, the nitrate concentration in ice should be used as an index of the nitrate air concentration. Dry deposition of HNO_3 forms a major pathway for the removal of inorganic nitrogen from the troposphere (Finlayson-Pitts and Pitts, 2000). In central Antarctica, nitrate is mainly deposited as gaseous HNO_3 (Legrand and Kirchner, 1990; Udisti *et al.*, 2004). From the point of view of the effect on the snow composition, this removal mechanism works as a peculiar dry deposition, since nitrate concentration is supposed to decrease as accumulation rate increases. For these reasons, the "cumulative dry deposition" (actual dry plus uptake of gaseous nitric acid) is expected to be more relevant for nitrate than wet deposition, even at a relatively high accumulation rate site like Talos Dome.

The directly measured quantity of nitrate content is its concentration NO_3(C) in ice. Nitrate flux (*i.e.*, the amount of nitrate falling upon a unit area per year) NO_3(F) cannot be measured directly, but is calculated as the product of the measured concentration and independently evaluated snow accumulation rate. For sites with dominantly dry deposition, flux

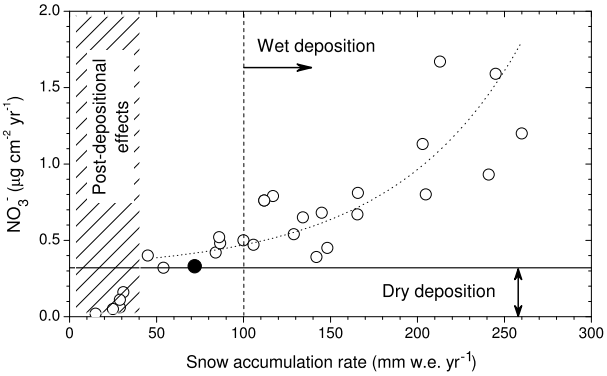

Figure 3 Relation between the nitrate flux and snow accumulation rate in different sites located in Northern Victoria Land of Antarctica and sampled along the ITASE traverse route towards Dome C (open circles). A roughly exponential dependence between the nitrate flux and the accumulation rate typical for wet deposition is illustrated by the dotted curve. The point corresponding to the Talos Dome site is depicted by the filled circle. The constant value of the nitrate flux corresponding to dry deposition is denoted by the solid horizontal line. Post-depositional effects are important at the sites with low snow accumulation rate. This region is indicated by the hatched bar. Contribution of wet deposition is important or dominant in the area right of the vertical dashed line.

is a more appropriate index of the atmospheric nitrate content, while concentration may be inversely modulated by the variable snow accumulation rate. For dominantly wet deposition conditions, on the contrary, the reconstruction of nitrate atmospheric concentration is not straightforward, since flux is expected to be directly modulated by the accumulation rate. The contribution of dry and wet deposition to the nitrate budget at the Talos Dome site can be assessed by analyzing the nitrate flux versus accumulation rate.

This is illustrated in Figure 3 showing the pattern of nitrate flux as a function of accumulation rate from sites located in Northern Victoria Land and sampled along the ITASE traverse route towards Dome C (open circles). For dry deposition, the flux should be constant (horizontal line) over a wide range of accumulation rate values. Sites with relatively low accumulation rates correspond to a dominant or exclusive dry deposition. However, at low accumulation rate below 50 mm w.e. (water equivalent) yr^{-1} (denoted by the hatched vertical bar), post-depositional effects may alter the nitrate content in ice as nitrate is not preserved (see discussion below). This makes the sites with low accumulation rate (mostly Antarctic inland) not useful for the present study. As the accumulation rate increases, the flux tends to increase (roughly exponentially) due to the progressively higher contribution of wet deposition. The flux values, to which the dependence on the accumulation rate asymptotically converges at low accumulation rates, but which are still high enough to avoid post-depositional effects, are considered as a reference value for dry deposition (Becagli *et al.*, 2005; Fischer and Wagenbach, 1996). At accumulation rates higher than 100 mm w.e. yr^{-1} (coastal sites) the contribution of wet deposition starts to be significant. Since wet deposition is driven by precipitation, it may be influenced by the local climate. Thus, an optimum site should be characterized by dominant dry deposition with a sufficiently high (50 – 100 mm w.e. yr^{-1}) snow accumulation rate to prevent post-depositional effects. The Talos Dome site (big solid circle in Figure 3) is indeed favorably located for long-term studies of its nitrate records. The average nitrate flux calculated for the TALDICE site in the Holocene [0.32 g cm^{-2} yr^{-1}] is comparable to the typical dry deposition value, suggesting a negligible contribution of wet deposition to nitrate deposition and the insensitivity of the nitrate flux

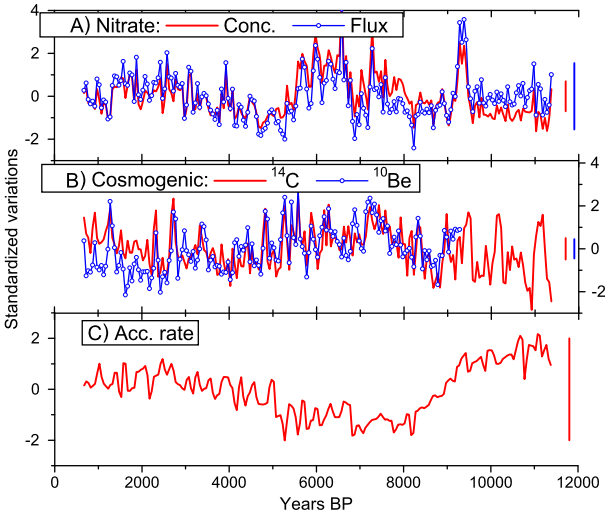

Figure 4 Time profiles of the standardized data series for the Holocene. Time is shown as BP (before present, where present is 1950 AD), with the most recent times on the left and increasing time meaning further in the past. Panel A: variations of the nitrate concentration (red curve) and flux (blue curve) at Talos Dome. Vertical bars on the right denote ranges of uncertainties (see Section 2.2): ≈ 10 % for concentration (red), and 18 % for flux (blue). Panel B: variability of the cosmic ray flux quantified as the count rate of a standard ground-based polar neutron monitor. Red and blue curves correspond to CR(^{14}C) and CR(^{10}Be) reconstructions, respectively. Uncertainties (see Section 2.1) of CR(^{14}C) and CR(^{10}Be) are 13 % and 10 % and indicated by the red and blue bars, respectively. Panel C: variation of the snow accumulation rate. The uncertainty (vertical bar) of 15 % (see Section 2.2) covers the entire range of variability, making it indistinguishable from a constant rate.

to possible long-term climate variations. On the other hand, local meteorological processes can still play a role on short time scales leading to "meteorological noise" in the annual data.

Although nitrate flux would be generally more appropriate for the nitrate content at Talos Dome, it is an indirectly calculated index, in contrast to the directly measured concentration. A very conservative estimate (Morganti *et al.*, 2007) of the possible NO_3(C) errors is below 10 %, composed of measurement errors (2 – 5 %) and systematic errors (<5 %). This is indicated by the red vertical bar in Figure 4A. Another factor required to calculate NO_3(F), the snow accumulation rate, is also known with uncertainties that are directly related to the ice core dating uncertainties of about 300 years for the Holocene (Schüpbach *et al.*, 2011). These timing errors are translated to the ± 15 % uncertainty (Buiron *et al.*, 2011) of the accumulation rate that covers the entire range of its variability over the Holocene (see the vertical bar in Figure 4C). Accordingly, the obtained snow accumulation rate is consistent, within the uncertainties, with a constant accumulation rate. Another source of uncertainty in the actual values of accumulation rate is related to changes in site elevation and in moisture origin areas experienced by TALDICE drilling site during the Holocene, directly affecting the accumulation rates derived from the isotopic record (Stenni *et al.*, 2011). The uncertainty, inherited by NO_3(F) from those of NO_3(C) and of snow accumulation rate, can be evaluated, assuming their independence, as ± 18 % (see the blue bar in Figure 4A), nearly double that of the nitrate concentration. In summary, the nitrate flux is more uncertain, because in addition to direct errors of the concentration measurements, it is affected by another important source of uncertainties – the dating errors.

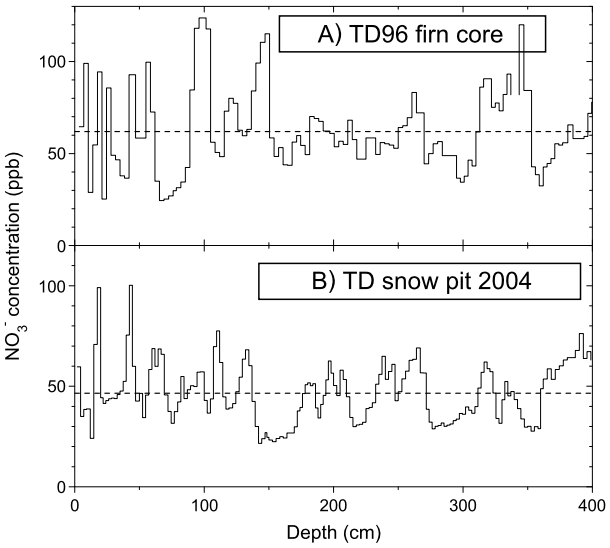

Figure 5 Nitrate concentration in the uppermost 4-m deep layers of two firn records from the Talos Dome site: a firn core TD96 and a snowpit excavated in 2004. The mean level is shown by the gray dashed line.

Variations of concentration and flux of a species are identical under the assumption of a constant accumulation rate, and such an assumption is valid for the Holocene in that variations in the accumulation rate lie below the uncertainties in this quantity. Accordingly, we consider here the concentration as a directly measured and more accurate quantity, over the indirectly calculated and thus more uncertain flux.

2.3. Nitrate Artifacts

Nitrate content in an ice core can be affected by post-depositional processes, which distort the original signal and hinder a direct atmospheric interpretation of the ice core NO_3 records (Grannas *et al.*, 2007). Here we discuss such processes in application to the Talos Dome record. Post-depositional effects may act via photolysis (Wolff, 1996; Dibb *et al.*, 2002), sublimation/condensation processes (Sturm and Benson, 1997) and uptake/release of volatile species (Legrand, Leopold, and Dominé, 1996). The key factors controlling nitrate loss are known and include snow accumulation rate, concentration in near surface air, site altitude and temperature and the presence of other species in snow (*e.g.*, Burkhart *et al.*, 2004), but their quantitative assessment is still insufficient (Röthlisberger *et al.*, 2000). At sites with low accumulation rate, where the most severe nitrate post-depositional loss takes place, snow layers remain close to the surface and/or in contact with the atmosphere for a relatively long time, enhancing the effect of the processes mentioned above. Several detailed studies (Wagnon, Delmas, and Legrand, 1999; Traversi *et al.*, 2009; Weller *et al.*, 2004) of post-depositional nitrate losses for Vostok and Dome C (East Antarctic plateau) and Kohnen Station (Dronning Maud Land) sites show that the nitrate concentration may drop, due to these effects, by about 90 % within the upper 50 – 80 cm at some sites in the Antarctic plateau.

Here we check the possible post-depositional effects for the Talos Dome site. Figure 5 shows the nitrate concentration as a function of depth in the uppermost 4-m layer at the Talos Dome site, as measured in the TD96 firn core (drilled in the 1996/1997 field season) and in a snowpit excavated in 2004, covering 20 years of snow deposition, corresponding to the 1977 – 1997 and 1984 – 2004 time periods, respectively. In both cases, no systematic

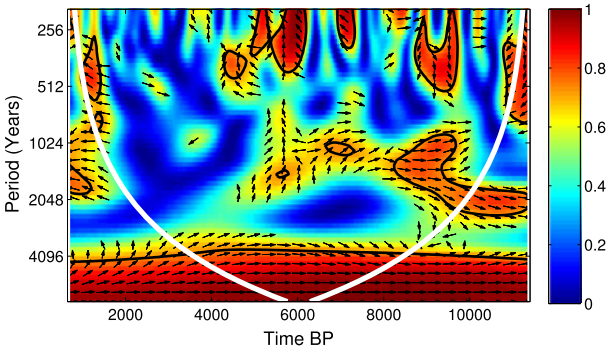

Figure 6 Wavelet coherence between NO_3(C) and CR(^{14}C) over the Holocene. Color (see the bar on the right) represents the coherence level. Contours bound areas with significant (95 % confidence level) coherence. The arrows denote the relative phasing between the two signals. The cone of influence (COI), where the wavelet spectrum may be distorted, is depicted by thick white lines.

decreasing trend can be observed with depth. The background values of around 50 ppb are consistent with the nitrate concentration throughout the whole Holocene in the TALDICE ice core and suggest that nitrate post-depositional effects are negligible at this site (see Section 2.2).

The average snow accumulation rate at Talos Dome, provided by TALDICE-1 dating (Buiron *et al.*, 2011), during the Holocene is 72.7 mm w.e. yr^{-1}, reaching a minimum of 60.9 mm w.e. yr^{-1} ca 5200 BP (see Figure 4C), still above the estimated threshold for post-depositional effects. The accumulation rate is rather stable, with only ± 7 % variability.

3. Results and Discussion

3.1. The Holocene Period

First we considered the data set covering the Holocene period (Figures 1 and 4): a simple visual comparison of the nitrate variability with the CR series yields similarities in the long-term trends, suggesting a possible relation with (inverted) solar activity. However, the visual inspection is inconclusive. A simple correlation gives the bivariate correlation coefficient $r = 0.27$, which is low but highly significant (the probability that it is due to a random coincidence is $p = 0.007$). The bivariate correlation between such noisy series is, however, dominated by the short-term fluctuations and does not tell much about longer time scales. In order to obtain a quantitative assessment of the agreement between the nitrate record and solar activity at different time scales, we applied to the raw data a wavelet coherence analysis, which determines both the magnitude, defined between 0 (no coherence) and 1 (full coherence), and the phase shift between the series, as a function of the frequency/timescale and time. Wavelet coherence is defined as the wavelet cross-spectrum of the two signals x and y, normalized to the power of the individual signals' spectra:

$$C_{xy}(f,t) = \frac{|W_{xy}(f,t)|^2}{W_{xx}(f,t) \cdot W_{yy}(f,t)}, \tag{1}$$

where W is the wavelet spectral density localized at frequency f and time t. Here we apply the commonly used Morlet basis (Grinsted, Moore, and Jevrejeva, 2004).

A plot of the wavelet coherence between the NO_3(C) and CR(^{14}C) is shown in Figure 6 for the whole Holocene. A stable, highly significant, perfectly in-phase coherence is observed at the multi-millennial time scale (red horizontal strip in the bottom). Intermittently significant coherence with fluctuating phase exists also at the millennial scale during the

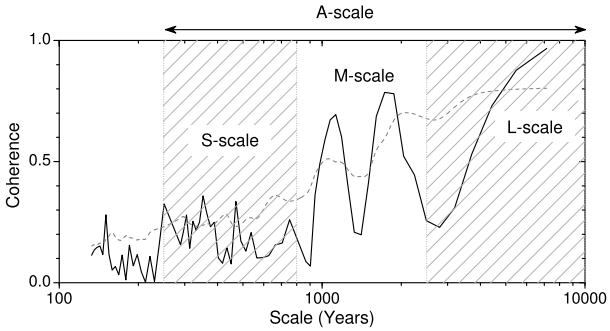

Figure 7 Time-integrated (outside COI) wavelet coherence spectrum for the NO_3(C) *vs.* CR(^{14}C) series (see Figure 6) as a function of the time scale/period. The gray dotted line depicts the 95 % confidence level calculated using the non-parametric random-phase method (see the Appendix). Vertical gray hatched bars are used to better distinguish between the time S- (250 – 800 yr), M- (800 – 2500 yr) and L- (> 2500 yr) scales, while the A-scale (> 250 yr) is indicated on the top of the panel.

early and mid-Holocene (orange to red areas at the time scale 1000 – 2000 years). Coherence on the multi-centennial scale is intermittent, and its stability and phase are unclear from a visual inspection.

Next we calculated the time-integrated wavelet coherence spectrum, which is the result of integration of the full 2D coherence spectrum (*e.g.*, Figure 6) over the time domain excluding COI (cone of influence). The COI is a region in the frequency domain, where the wavelet spectrum can be distorted by the edges of the time series and thus should not be used (see Grinsted, Moore, and Jevrejeva, 2004). The corresponding spectrum in the frequency domain is shown in Figure 7. For a more detailed analysis we roughly divided the whole time scale into sub-scales: short (S) scale stands for sub-millennial time scale of 250 – 800 years; millennial (M) time scale 800 – 2500 years; and long (L) scale for multi-millennial scale longer than 2500 years. Amalgamated (A) scale stands for the entire time scale longer than 300 years, *i.e.* above the dating uncertainties in the nitrate series. In order to obtain a quantitative measure of the agreement between the series in the appropriate time scale, we use the integral coherence calculated in the frequency bands corresponding to the time scale considered. This gives the magnitude C and the relative phasing of the coherence for each pair of time series. We also estimate the significance p of the obtained coherence (the chance that it is due to a random coincidence) using the random-phase non-parametric method (see the Appendix). Here we also considered the relative phasing between the series: only coherences with the relative phasing within $\pm\pi/4$ or with the absolute time difference less than 300 years were considered, while coherences with larger phase differences were set to zero. The results are shown in Table 1. We note that all the integrated coherences have been calculated from the raw data, without any filtering or smoothing, applying integration in the time and frequency domains to the full 2D wavelet coherence spectrum.

First block of Table 1 (rows 1–4) presents integral coherences between the series discussed here. In order to visualize these relations, we plotted in Figure 3 the time series of NO_3(C), CR(^{14}C) and CR(^{10}Be), filtered over the appropriate time scales, which is done solely for illustration and has no evidential power. Multi-millennial variabilities (L-scale, panel A) of NO_3(C) and CR(^{14}C) agree well with each other, while CR(^{10}Be) differs from both. At the M-scale (panel B), the agreement between all the series is good, but the relative phasing and amplitude of the peaks vary somewhat. At the S-scale (panel C), the pattern is indistinct, although some periods of agreement are apparent.

Table 1 Integral coherence calculated in the frequency bands corresponding to the considered time scales (see main text). The coherence and its significance (in parentheses) are estimated by the non-parametric random-phase method (see the Appendix). The relative shift between the time series is always less than 300 years. Significant coherences (significance of 0.05 or better) are highlighted in italic face. Highly significant coherences (0.01 or better) are printed in bold face.

Data series	L-scale	M-scale	S-scale	A-scale
(1) NO_3(C) *vs.* CR(^{14}C)	**0.53** ($< 10^{-3}$)	**0.28** (0.003)	*0.20* (0.02)	**0.27** ($< 10^{-3}$)
(2) NO_3(C) *vs.* CR(^{10}Be)	*0.36* (0.02)	**0.36** ($< 10^{-3}$)	*0.24* (0.02)	**0.29** ($< 10^{-3}$)
(3) NO_3(F) *vs.* CR(^{14}C)	*0.36* (0.04)	**0.28** (0.002)	*0.20* (0.04)	**0.23** (0.006)
(4) NO_3(F) *vs.* CR(^{10}Be)	0.1 (0.7)	**0.32** (0.01)	*0.21* (0.05)	**0.23** (0.01)
(5) NO_3(F) *vs.* NO_3(C)	**0.83** ($< 10^{-3}$)	**0.95** ($< 10^{-3}$)	**0.87** ($< 10^{-3}$)	**0.90** ($< 10^{-3}$)
(6) CR(^{14}C) *vs.* CR(^{10}Be)	*0.32* (0.03)	**0.33**(0.01)	**0.43** ($< 10^{-3}$)	**0.38** ($< 10^{-3}$)
(7) NO_3(C) *vs.* δ^{18}O	0.08 (> 0.5)	0.08 (> 0.5)	0.19 (0.12)	0.15 (0.34)
(8) NO_3(C) *vs.* MSA	0.15 (0.43)	0.16 (0.4)	0.12 (> 0.5)	0.14 (> 0.5)
(9) NO_3(C) *vs.* Ca	0.20 (0.26)	0.05 (> 0.5)	0.19 (0.12)	0.13 (> 0.5)
(10) NO_3(C) *vs.* Na	0.12 (> 0.5)	0.07 (> 0.5)	0.14 (> 0.5)	0.11 (> 0.5)

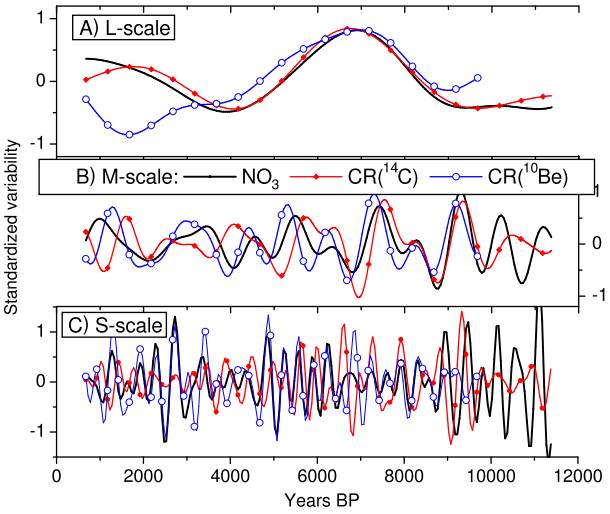

Figure 8 Variations of the nitrate concentration (solid black) as well as ^{14}C- (red) and ^{10}Be-based (blue) cosmic ray reconstructions filtered, using wavelet digital filters, in selected time scales: L-scale (panel A) represents the multi-centennial variability (low-pass filter > 3000 years); M-scale (panel B) represents the millennial scale variability (band-pass filter 1000 – 2000 years); S-scale (panel C) represents the sub-millennial variability (band-pass filter 300 – 700 years). We do not consider time scales below 300 years due to the dating uncertainty in the nitrate time series (Schüpbach *et al.*, 2011).

At the multi-millennial L-scale (second column of Table 1 and Figure 8A), only the NO_3(C)–CR(^{14}C) pair (row 1) shows highly significant coherence ($C = 0.53$, *i.e.* 30 % common variability, $p = 0.001$). Other combinations give barely significant (rows 2 and 3) or no coherence (row 4). CR(^{10}Be) shows lower or no coherence with both nitrate indices and CR(^{14}C). We note that the L-scale coherence between ^{10}Be and ^{14}C is low and barely significant, reflecting the discrepancy between the two cosmogenic records in the early Holocene (Vonmoos, Beer, and Muscheler, 2006; Usoskin *et al.*, 2009). The agreement between the nitrate and ^{14}C records is much better at this time scale.

All the pair-wise coherences at the millennial M-scale (third column of Table 1 and Figure 8B) are highly significant pointing to a common source of variability at this time scale. CR *vs.* nitrate indices show a similar level of coherence as between the two cosmogenic data sets. NO_3(C) and NO_3(F) are nearly identical at the M-scale.

The pair-wise coherence at the centennial S-scale (fourth column of Table 1 and Figure 8C) is not high and barely significant for all pairs, which is related to the dating uncertainties of the nitrate series. Both CR(^{10}Be) and CR(^{14}C) covary with nitrate at this time scale, with slightly better coherence for CR(^{10}Be), in agreement with earlier results obtained from a shallow ice core (Laluraj *et al.*, 2010). Pairs, for which the dating uncertainties are not involved, viz. NO_3(C) *vs.* NO_3(F) and CR(^{14}C) *vs.* CR(^{10}Be), are listed in the second block of Table 1 (rows 5 – 6). The coherence within these pairs is higher and much more significant than for those pairs where the relative dating between the series can be uncertain.

All the coherences at the A-scale (fifth column of Table 1) are highly significant for both the first and the second blocks, suggesting a strong common source of variability between the analyzed records. We want to emphasize that the agreement between CR and nitrate indices is similar to or better than that between the two cosmogenic records at millennial and multi-millennial time scales.

We have additionally studied, in the same manner, relations between the nitrate concentration and various auxiliary indices measured in the same TALDICE ice core, including δ^{18}O (local/regional climate), MSA (marine biogenic activity), Ca (mineral dust input), and Na (sea spray transport processes and/or sea ice extent; Wolff *et al.*, 2010; Udisti *et al.*, 2012). Since they are measured in the same core, dating uncertainties do not affect the coherences between them. The corresponding integral coherences are shown in the third block of Table 1 (rows 7 – 10). None of the indices is coherent with the nitrate record, suggesting that the local/regional climate and transport do not affect the nitrate content at Talos Dome at centennial-millennial time scales. At the S-scale, the coherence between NO_3(C) and δ^{18}O and between NO_3(C) and Ca(C) is lower than that calculated between NO_3(C) and NO_3(F) and the cosmogenic isotopes (first block of Table 1) and insignificant (0.12 *vs.* 0.02 – 0.05). A similar result (no significant coherence, not shown in Table 1) is found between CR records and these auxiliary indices (δ^{18}O, MSA, Ca, Na). On the other hand, the integral coherence between these auxiliary indices (not shown) is highly significant, suggesting that they are strongly inter-related.

In summary, the new marker, the nitrate content (both concentration and flux) in the Talos Dome ice core, exhibits a good and highly significant agreement with the ^{14}C-based CR reconstruction, on millennial and multi-millennial time scales over the Holocene. Considering the very different mechanisms of their production and transport/redistribution in the geosphere, this suggests that they both are dominated by the same external process, viz. solar activity. The hypothetical possibility that they are linked via an unknown long-term climatic change (*e.g.*, of the ocean circulation around Antarctica) can be discarded based on the analysis of auxiliary data (δ^{18}O, MSA, Na, Ca from the same ice core), tracing the local/regional climate/transport, as discussed above. No significant relation was found between the nitrate record from TALDICE and the geomagnetic field, quantified via the virtual aligned dipole moment (VADM) over the Holocene (Knudsen *et al.*, 2008; Korte *et al.*, 2011). This suggests that nitrate deposited in the Antarctic ice is most likely produced locally, in the polar region, where CRs are not shielded by the geomagnetic field. Therefore, the polar production term driven by solar variability is expected to contribute to the nitrate record. The results for the Holocene period can be summarized as follows.

- All analyzed pairs of CR and nitrate indices depict highly significant coherence at millennial and amalgamated time scales.
- At the multi-millennial time scale only the NO_3(C) *vs.* CR(^{14}C) pair shows highly significant coherence, which is higher than that between the two cosmogenic records, ^{14}C and ^{10}Be.

– All pair-wise coherences between CR and nitrate indices are barely significant at the centennial scale, being affected by the dating uncertainties in the ice core.
– No coherence is found between the nitrate or CR series and the local/regional climate/transport markers.

3.2. 11-year and Gleissberg Solar Cycle in Nitrate Data

Next we checked if a relationship between the Talos Dome nitrate record and solar activity exists on the sub-centennial time scale, including the 11-yr solar cycle and the Gleissberg cycle. We focused on the last centuries, when the solar activity record is well documented through direct sunspot observations. Solar cycles are more or less reliably known after the Maunder minimum (Usoskin, 2008), with regular cycles started ca. 1713. For the analysis we used the nitrate concentration measured with sub-annual resolution in the TALDICE firn samples, averaged to annual data (Figure 2A). In order to verify the consistency of the results we consider two time intervals here. One is limited to the pre-industrial epoch, 1713 – 1913 AD, covering 18 solar cycles, Nos. − 3 to 14 in Zurich numeration. Although 1913 AD corresponds to rapid industrialization in the Northern hemisphere, it can still be considered as pre-industrial in the Southern hemisphere. It is characterized by low-to-moderate solar activity and should be without the potential influence of anthropogenic nitrate sources, which is difficult to account for (Savarino *et al.*, 2007). The other period is 1713 – 1981 AD, which includes also a strong rise of solar activity in the first half of 20th century and possible anthropogenic factors. Solar variability is represented by the annual GCR flux reconstructed from sunspot data (see Section 2.1 and Figure 2B), similarly to Usoskin *et al.* (2002) but using a recent solar open flux model (Krivova, Balmaceda, and Solanki, 2007; Vieira and Solanki, 2010; Vieira *et al.*, 2011).

A visual inspection is inconclusive because of the noisy nitrate data at interannual scale (bivariate correlation $r = 0.17$ is low and only weakly significant, $p = 0.06$). The bivariate correlation, however, is dominated by the short-term fluctuations (meteorological noise – see Section 2.2) rather than the smooth 11-year cyclic changes. This makes it hardly possible to distinguish individual solar cycles in the nitrate data (Weller *et al.*, 2011), and a signature of the 11-year cycle can be found only in a statistical refined sense. This is similar to the ^{10}Be data, which are a widely recognized index of CR and solar activity on decadal and longer time scales (*e.g.*, Beer *et al.*, 1990): the coefficient of bivariate linear correlation between annual raw ^{10}Be (Dye-3; Beer *et al.*, 1990) and CR data is only 0.14, viz. even less than that for nitrate data, and the meteorological noise can greatly affect the ^{10}Be data up to the time scale of several decades (Usoskin *et al.*, 2009). Individual solar cycles are also hardly recognizable in the raw ^{10}Be data without filtering (Beer *et al.*, 1990).

In order to obtain a quantitative assessment of the agreement between the nitrate record and CR, we again applied a wavelet coherence analysis to the raw data in the same way as described in Section 3.1. The reliable period range is from 3 – 5 years (limited by the dating uncertainties) to about 100 years (limited by the length of the analyzed series). This includes two distinct solar cycles: the Schwabe 11-year cycle, and the Gleissberg cycle which has a characteristic time scale of 60 – 120 years (Ogurtsov, 2004). We have calculated the integral coherence in the frequency bands corresponding to the 11-yr cycle (7 – 15 years), Gleissberg cycle (55 – 100 years) and the entire time scale (5 – 100 years) as summarized in Table 2. One can see that coherences in all the frequency bands are highly significant for the pre-industrial epoch (1713 – 1913). In particular, the coherence in the 11-yr cycle band is ≈ 0.3 (nitrate is 0.5 – 1 years delayed with respect to CR), which implies 7 – 10 % of common variability. We note that the meteorological noise, dominant at the interannual time scale,

Table 2 Integral coherence between the annual Talos Dome firn nitrate series and cosmic rays for two time intervals, as calculated in the frequency bands corresponding to the 11-yr solar cycle (7 – 15 years), Gleissberg cycle (55 – 100 years) and the entire scale (5 – 100 years). The coherence and its significance (in parentheses) are estimated by the non-parametric random-phase method (see the Appendix). Significant coherences (significance of 0.05 or better) are highlighted in italic face. Highly significant coherences (0.01 or better) are printed in bold face.

Time interval	7 – 15 yr	55 – 100 yr	5 – 100 yr
1713 – 1913	**0.31** (0.01)	**0.6** (0.01)	**0.24** (0.01)
1713 – 1981	*0.24* (0.03)	*0.49* (0.02)	*0.20* (0.03)

makes individual 11-yr cycles hardly distinguishable in the nitrate data (see Figure 2A). When the 20th century is included into the analysis (1713 – 1981) the coherence becomes less significant, most likely because of the growing anthropogenic source of nitrate. The coherence in the Gleissberg cycle band is higher 0.5 – 0.6 (relative phasing is within 1 year), implying about 25 % common variability, because the meteorological noise is less important at the decadal scale. The use of (inverted) sunspot numbers instead of CR or nitrate flux instead of concentration does not alter the conclusion. Thus, there is a statistically significant in-phase relation between nitrate in the TALDICE firn core and CR variability at the interannual-decadal time scale including the solar 11-yr and the Gleissberg cycles. This agrees with the results by Laluraj *et al.* (2010) who found an agreement between nitrate and ^{10}Be data measured in a shallow Antarctic ice core for the last 450 years.

Because of the complicated transport/deposition process of nitrate in the polar atmosphere, a full model including both production and transport/deposition of nitrate is needed in order to understand the process. To the best of our knowledge, such a complete model is presently missing. However, some estimates of the expected relation can be made on the basis of existing model simulations. Several model experiments have been performed, computing the effect of GCR in NO_y/HNO_3 concentration in the atmosphere for the modern epoch, using independent models SOCOL (Calisto *et al.*, 2011; Rozanov *et al.*, 2012) and CMAM (Semeniuk *et al.*, 2011). Both models predict a 20 – 30 % on-off effect of GCR in HNO_3 and NO_y in near-ground air in Antarctica, while no observable effect is expected in the Arctic region (Greenland). A dedicated model simulation is pending.

The results for the sub-centennial time scale are:

– Highly significant in-phase coherence between nitrate concentration in the Talos Dome firn record and cosmic ray reconstructions for the pre-industrial epoch exists in the time scale covering the 11-yr and Gleissberg cycles. This suggests a 10 – 20 % common variability which is consistent with the existing model simulations. However, a dedicated model needs to be developed.
– The relation weakens in the 20th century, likely due to the growing anthropogenic contribution to nitrate variability.

4. Conclusions

We have compared the nitrate record in the Talos Dome site with two commonly used proxies of solar variability, cosmogenic nuclide data of ^{14}C in trees (Stuiver and Braziunas, 1989; Reimer *et al.*, 2004) and ^{10}Be in polar ice (Beer *et al.*, 1990; Steinhilber, Abreu, and Beer, 2008).

We found that the nitrate data exhibit highly significant agreement with the cosmic ray flux reconstructions on the millennial and multi-millennial time scales throughout the Holocene (Section 3.1). The relation at centennial time scales is less significant since it is complicated by dating uncertainties. The two proxy records have different production and transport patterns: *e.g.*, ^{14}C data, used as a proxy for cosmic rays in the past, is produced globally, mixed in the geosphere, and is mostly affected by ocean circulation; nitrate in the Antarctic polar region is produced mostly locally and can be affected by regional Antarctic air transport. No statistical relationship was found between the nitrate data and the regional climatic markers. Consequently, the coherence between nitrate and cosmogenic isotopes univocally suggests a common origin of their long-term variability. We have also found a significant in-phase relation between nitrate in the firn core from the Talos Dome and cosmic rays on the interannual and multi-decadal time scale in the pre-industrial epoch after the Maunder minimum, which is in agreement with model results (Section 3.2). Therefore, we conclude that nitrate in the Antarctic ice core forms a novel proxy of solar activity on the centennial and longer time scales, which may resolve some of the discrepancy to the other records.

The relation between nitrate and ^{10}Be-based data is also significant at millennial and sub-millennial time scales, but is weak at the multi-millennial time scale. This may be due to the fact that transport of ^{10}Be is characterized by partial atmospheric mixing and sensitivity to polar climate. Nitrate depicts better agreement with CR(^{14}C) at the multi-millennial time scale than with ^{10}Be, supporting solar activity reconstructions based on radiocarbon on the longer time scales.

We have established nitrate as a solar activity proxy for the Holocene, but it may potentially be applicable also to the last glacial period, when the long-term variation of the cosmogenic isotope proxies becomes uncertain because of the severe climate changes.

We note that the Talos Dome site is favorably located to minimize possible local climate effects, which may be dominant in other coastal sites. Moreover, due to a sufficiently high snow accumulation rate, such a reversibly deposited species as nitrate is preserved at Talos Dome (in contrast to inland Antarctic sites) making it a potential paleomarker.

For future work, including a quantitative reconstruction of solar activity based on nitrate records, the production and transport of nitrate need to be properly modeled. Such modeling has been initiated.

Acknowledgements This work is a contribution to the TALDICE and HOLOCLIP projects. TALDICE (Talos Dome Ice Core Project) is a joint European programme, funded by national contributions from Italy, France, Germany, Switzerland and the United Kingdom. Primary logistic support was provided by PNRA at Talos Dome. HOLOCLIP is a joint research project of ESF PolarCLIMATE programme, funded by national contributions from Italy, France, Germany, Spain, Netherlands, Belgium, and the United Kingdom. This is TALDICE publication n. 21. This is HOLOCLIP publication No. 10. This work has been partly supported by WCU grant No. R31-10016 of the Korean Ministry of Education, Science and Technology.

Appendix: Non-parametric Random Phase Method to Estimate the Significance of Coherence

When discussing any statistical measures of agreement between time series, such as correlation or coherence, not only the magnitude but also the significance should be calculated, which evaluates the probability that the correlation/coherence is caused by a random coincidence. This is particularly important for pre-processed (*e.g.*, smoothed, filtered, or detrended) series where the standard formulas of error propagation are not directly applicable.

In addition, standard significance estimates are usually based on the assumption that the data are subject to normally distributed additive random white noise. However, this assumption is often violated because of significant autocorrelation within the actual data series. This is of particular relevance for the long-term changes studied here. In such a situation, a Monte-Carlo test can be applied to estimate the significance of the calculated coherence.

A simple random shuffling of the real data series, which is sometimes applied, typically leads to a serious overestimate of the significance because it destroys the serial correlation (Usoskin *et al.*, 2006a). Here we applied a non-parametric random-phase method, as described below, suggested by Ebisuzaki (1997) and successfully applied in many studies of various physical systems.

Let us denote the two analyzed time series as x and y, with the coherence being C_{xy}. The significance estimate is performed as follows.

i) The x series is randomized by the random-phase method: first, the FFT-transform f of the original x series is computed, $x \xrightarrow{(\mathrm{FFT})} f$; in a second step, a new FFT f' series is produced which has the same amplitude as the f-series but whose phase sequence is randomized, $f \xrightarrow{(\mathrm{rand.phase})} f'$; thirdly, the new phase-randomized x' series is obtained by an inverse FFT-transform of the f' series, $f' \xrightarrow{(\mathrm{FFT}^{-1})} x'$.
ii) The new value of the coherence is calculated between the phase-randomized x' and the original y series, $C_{x'y}$.
iii) A phase-randomized y' series of the y series is produced in the same way as described in item 1 above, and the coherence $C_{xy'}$ is calculated.
iv) The maximum of $C_{x'y}$ and $C_{xy'}$ is considered as C^*.
v) Steps 1 – 4 are repeated N times to obtain a sequences of C^* values. Then the number N^* is calculated, which is the number of cases (within the total of N simulations) when C^* exceeds C_{xy} in the absolute value, within the defined relative phase range.

Finally, the significance is defined as

$$s = N^*/N \tag{2}$$

and gives an estimate of the chance that the observed coherence level is not due to a causal relationship but is rather produced by a random coincidence. Here we used the number of random realizations $N = 10^5$. An example in Figure 7 shows the calculated integral coherence between NO_3(C) and CR(^{14}C) series, as a function of the time scale, and its 95 % confidence level. This method, called the non-parametric random-phase test, preserves the autocorrelation function of the original series. Moreover, this method may tend to underestimate the confidence level (*i.e.*, overestimate the probability of a random coincidence) if one of the time series is dominated by a periodic signal (Usoskin *et al.*, 2006a). Thus, we consider this significance estimate as conservative.

References

Bard, E., Raisbeck, G.M., Yiou, F., Jouzel, J.: 1997, *Earth Planet. Sci. Lett.* **150**, 453.
Becagli, S., Proposito, M., Benassai, S., Flora, O., Genoni, L., Gragnani, R., Largiuni, O., Pili, S.L., Severi, M., Stenni, B., Traversi, R., Udisti, R., Frezzotti, M.: 2004, *Ann. Glaciol.* **39**, 473.
Becagli, S., Proposito, M., Benassai, S., Gragnani, R., Magand, O., Traversi, R., Udisti, R.: 2005, *Ann. Glaciol.* **41**, 23.
Beer, J., Blinov, A., Bonani, G., Hofmann, H.J., Finkel, R.C.: 1990, *Nature* **347**, 164.

Buiron, D., Chappellaz, J., Stenni, B., Frezzotti, M., Baumgartner, M., Capron, E., Landais, A., Lemieux-Dudon, B., Masson-Delmotte, V., Montagnat, M., Parrenin, F., Schilt, A.: 2011, *Clim. Past* **7**, 1.
Burkhart, J.F., Hutterli, M., Bales, R.C., McConnell, J.R.: 2004, *J. Geophys. Res.* **109**, D19302.
Calisto, M., Usoskin, I., Rozanov, E., Peter, T.: 2011, *Atmos. Chem. Phys.* **11**, 4547.
Charbonneau, P.: 2010, *Living Rev. Solar Phys.* **7**(3). http://www.livingreviews.org/lrsp-2010-3.
de Jager, C.: 2005, *Space Sci. Rev.* **120**, 197.
Dibb, J.E., Arsenault, M., Peterson, M.C., Honrath, R.E.: 2002, *Atmos. Environ.* **36**, 2501.
Dorman, L.I.: 2004, *Cosmic Rays in the Earth's Atmosphere and Underground*, Kluwer Academic, Dordrecht, 485.
Ebisuzaki, W.: 1997, *J. Climate* **10**, 2147.
Eddy, J.A.: 1976, *Science* **192**, 1189.
Egorova, T., Rozanov, E., Ozolin, Y., Shapiro, M., Calisto, Y., Peter, T., Schmutz, W.: 2011, *J. Atmos. Solar-Terr. Phys.* **73**, 356.
Finkel, R.C., Nishiizumi, K.: 1997, *J. Geophys. Res.* **102**, 26699.
Finlayson-Pitts, B., Pitts, J.N.J.: 2000, *Chemistry of the Upper and Lower Atmosphere: Theory, Experiments, and Applications*, Academic Press, San Diego, 32.
Fischer, H., Wagenbach, D.: 1996, *Atmos. Environ.* **30**, 3227.
Grannas, A.M., Jones, A.E., Dibb, J., Ammann, M., Anastasio, C., Beine, H.J., Bergin, M., Bottenheim, J., Boxe, C.S., Carver, G., Chen, G., Crawford, J.H., Dominé, F., Frey, M.M., Guzmán, M.I., Heard, D.E., Helmig, D., Hoffmann, M.R., Honrath, R.E., Huey, L.G., Hutterli, M., Jacobi, H.W., Klán, P., Lefer, B., McConnell, J., Plane, J., Sander, R., Savarino, J., Shepson, P.B., Simpson, W.R., Sodeau, J.R., von Glasow, R., Weller, R., Wolff, E.W., Zhu, T.: 2007, *Atmos. Chem. Phys.* **7**, 4329.
Gray, L.J., Beer, J., Geller, M., Haigh, J.D., Lockwood, M., Matthes, K., Cubasch, U., Fleitmann, D., Harrison, G., Hood, L., Luterbacher, J., Meehl, G.A., Shindell, D., van Geel, B., White, W.: 2010, *Rev. Geophys.* **48**, RG4001.
Grinsted, A., Moore, J.C., Jevrejeva, S.: 2004, *Nonlinear Process. Geophys.* **11**, 561.
Honrath, R.E., Peterson, M.C., Guo, S., Dibb, J.E., Shepson, P.B., Campbell, B.: 1999, *Geophys. Res. Lett.* **26**, 695.
Kepko, L., Spence, H., Smart, D.F., Shea, M.A.: 2009, *J. Atmos. Solar-Terr. Phys.* **71**, 1840.
Knudsen, M.F., Riisager, P., Donadini, F., Snowball, I., Muscheler, R., Korhonen, K., Pesonen, L.J.: 2008, *Earth Planet. Sci. Lett.* **272**, 319.
Korte, M., Constable, C., Donadini, F., Holme, R.: 2011, *Earth Planet. Sci. Lett.* **312**, 497.
Krivova, N.A., Balmaceda, L., Solanki, S.K.: 2007, *Astron. Astrophys.* **467**, 335.
Lal, D.: 2007, *Earth Planet. Sci. Lett.* **264**, 177.
Laluraj, C.M., Thamban, M., Naik, S.S., Redkar, B.L., Chaturvedi, A., Ravindra, R.: 2010, *Holocene* **21**, 351.
Legrand, M.R., Kirchner, S.: 1990, *J. Geophys. Res.* **95**, 3493.
Legrand, M., Mayewski, P.: 1997, *Rev. Geophys.* **35**, 219.
Legrand, M., Leopold, A., Dominé, F.: 1996, In: Wolff, E.W., Bales, R.C. (eds.) *Processes of Chemical Exchange Between the Atmosphere and Polar Snow*, *NATO ASI Series I* **43**, Springer, Berlin, 19.
McCracken, K.G., Beer, J.: 2007, *J. Geophys. Res.* **112**, A10101.
Morganti, A., Becagli, S., Castellano, E., Severi, M., Traversi, R., Udisti, R.: 2007, *Anal. Chim. Acta* **603**, 190.
Nandy, D., Muñoz-Jaramillo, A., Martens, P.C.H.: 2011, *Nature* **471**, 80.
Ogurtsov, M.G.: 2004, *Solar Phys.* **220**, 93.
Oppo, D.W., McManus, J.F., Cullen, J.L.: 2003, *Nature* **422**, 277.
Reimer, P.J., Baillie, M.G.L., Bard, E., Bayliss, A., Beck, J.W., Bertrand, C.J.H., Blackwell, P.G., Buck, C.E., Burr, G.S., Cutler, K.B., Damon, P.E., Edwards, R.L., Fairbanks, R.G., Friedrich, M., Guilderson, T.P., Hogg, A.G., Hughen, K.A., Kromer, B., McCormac, G., Manning, S., Ramsey, C.B., Reimer, R.W., Remmele, S., Southon, J.R., Stuiver, M., Talamo, S., Taylor, F.W., van der Plicht, J., Weyhenmeyer, C.E.: 2004, *Radiocarbon* **46**, 1029.
Röthlisberger, R., Hutterli, M.A., Sommer, S., Wolff, E.W., Mulvaney, R.: 2000, *J. Geophys. Res.* **105**, 20565.
Rozanov, E., Calisto, M., Egorova, T., Peter, T., Schmutz, W.: 2012, *Surv. Geophys.* **33**, 483.
Savarino, J., Kaiser, J., Morin, S., Sigman, D.M., Thiemens, M.H.: 2007, *Atmos. Chem. Phys.* **7**, 1925.
Schüpbach, S., Federer, U., Bigler, M., Fischer, H., Stocker, T.F.: 2011, *Clim. Past* **7**, 1001.
Semeniuk, K., Fomichev, V.I., McConnell, J.C., Fu, C., Melo, S.M.L., Usoskin, I.G.: 2011, *Atmos. Chem. Phys.* **11**, 5045.
Severi, M., Udisti, R., Becagli, S., Stenni, B., Traversi, R.: 2012, *Clim. Past* **8**, 509.
Shea, M.A., Smart, D.F., McCracken, K.G., Dreschhoff, G.A.M., Spence, H.E.: 2006, *Adv. Space Res.* **38**, 232.
Snowball, I., Muscheler, R.: 2007, *Holocene* **17**, 851.

Solanki, S.K., Usoskin, I.G., Kromer, B., Schüssler, M., Beer, J.: 2004, *Nature* **431**, 1084.
Steig, E.J., Polissar, P.J., Stuiver, M., Grootes, P.M., Finkel, R.C.: 1996, *Geophys. Res. Lett.* **23**, 523.
Steinhilber, F., Abreu, J.A., Beer, J.: 2008, *Astrophys. Space Sci. Trans.* **4**, 1.
Stenni, B., Proposito, M., Gragnani, R., Flora, O., Jouzel, J., Falourd, S., Frezzotti, M.: 2002, *J. Geophys. Res.* **107**, 4076.
Stenni, B., Buiron, D., Frezzotti, M., Albani, S., Barbante, C., Bard, E., Barnola, J.M., Baroni, M., Baumgartner, M., Bonazza, M., Capron, E., Castellano, E., Chappellaz, J., Delmonte, B., Falourd, S., Genoni, L., Iacumin, P., Jouzel, J., Kipfstuhl, S., Landais, A., Lemieux-Dudon, B., Maggi, V., Masson-Delmotte, V., Mazzola, C., Minster, B., Montagnat, M., Mulvaney, R., Narcisi, B., Oerter, H., Parrenin, F., Petit, J.R., Ritz, C., Scarchilli, C., Schilt, A., Schüpbach, S., Schwander, J., Selmo, E., Severi, M., Stocker, T.F., Udisti, R.: 2011, *Nat. Geosci.* **4**, 46.
Stuiver, M., Braziunas, T.F.: 1989, *Nature* **338**, 405.
Stuiver, M., Reimer, P.J., Bard, E., Burr, G.S., Hughen, K.A., Kromer, B., McCormac, G., v.d. Plicht, J., Spurk, M.: 1998, *Radiocarbon* **40**, 1041.
Sturm, M., Benson, C.S.: 1997, *J. Glaciol.* **43**, 42.
Traversi, R., Becagli, S., Castellano, E., Migliori, A., Severi, M., Udisti, R.: 2002, *Ann. Glaciol.* **35**, 291.
Traversi, R., Becagli, S., Castellano, E., Largiuni, O., Migliori, A., Severi, M., Frezzotti, M., Udisti, R.: 2004, *Int. J. Environ. Anal. Chem.* **84**, 457.
Traversi, R., Becagli, S., Castellano, E., Cerri, O., Morganti, A., Severi, M., Udisti, R.: 2009, *Microchem. J.* **92**, 7.
Udisti, R., Becagli, S., Benassai, S., Castellano, E., Fattori, I., Innocenti, M., Migliori, A., Traversi, R.: 2004, *Ann. Glaciol.* **39**, 53.
Udisti, R., Dayan, U., Becagli, S., Busetto, M., Frosini, D., Legrand, M., Lucarelli, F., Preunkert, S., Severi, M., Traversi, R., Vitale, V.: 2012, *Atmos. Environ.* **52**, 109.
Usoskin, I.G.: 2008, *Living Rev. Solar Phys.* **5**(3). http://www.livingreviews.org/lrsp-2008-3.
Usoskin, I.G., Solanki, S.K., Kovaltsov, G.A.: 2007, *Astron. Astrophys.* **471**, 301.
Usoskin, I.G., Mursula, K., Solanki, S.K., Schüssler, M., Kovaltsov, G.A.: 2002, *J. Geophys. Res.* **107**, 1374.
Usoskin, I.G., Alanko-Huotari, K., Kovaltsov, G.A., Mursula, K.: 2005, *J. Geophys. Res.* **110**, A12108.
Usoskin, I.G., Voiculescu, M., Kovaltsov, G.A., Mursula, K.: 2006a, *J. Atmos. Solar-Terr. Phys.* **68**, 2164.
Usoskin, I.G., Solanki, S.K., Kovaltsov, G.A., Beer, J., Kromer, B.: 2006b, *Geophys. Res. Lett.* **33**, L08107.
Usoskin, I.G., Horiuchi, K., Solanki, S., Kovaltsov, G.A., Bard, E.: 2009, *J. Geophys. Res.* **114**, A03112.
Vieira, L.E.A., Solanki, S.K.: 2010, *Astron. Astrophys.* **509**, A100.
Vieira, L.E.A., Solanki, S.K., Krivova, N.A., Usoskin, I.: 2011, *Astron. Astrophys.* **531**, A6.
Vonmoos, M., Beer, J., Muscheler, R.: 2006, *J. Geophys. Res.* **111**, A10105.
Wagnon, P., Delmas, R.J., Legrand, M.: 1999, *J. Geophys. Res.* **104**, 3423.
Weller, R., Traufetter, F., Fischer, H., Oerter, H., Piel, C., Miller, H.: 2004, *J. Geophys. Res.* **109**, D07301.
Weller, R., Wagenbach, D., Legrand, M., Elsńsser, C., Tian-Kunze, X., Kónig-Langlo, G.: 2011, *Tellus B* **63**, 901.
Wolff, E.W.: 1996, *J. Geophys. Res.* **101**, 27735.
Wolff, E.W., Jones, A.E., Bauguitte, S.J.-B., Salmon, R.A.: 2008, *Atmos. Chem. Phys.* **8**, 5627.
Wolff, E.W., Barbante, C., Becagli, S., Bigler, M., Boutron, C.F., Castellano, E., de Angelis, M., Federer, U., Fischer, H., Fundel, F., Hansson, M., Hutterli, M., Jonsell, U., Karlin, T., Kaufmann, P., Lambert, F., Littot, G.C., Mulvaney, R., Röthlisberger, R., Ruth, U., Severi, M., Siggaard-Andersen, M.L., Sime, L.C., Steffensen, J.P., Stocker, T.F., Traversi, R., Twarloh, B., Udisti, R., Wagenbach, D., Wegner, A.: 2010, *Quat. Sci. Rev.* **29**, 285.
Wolff, E.W., Bigler, M., Curran, M., Dibb, J.E., Frey, M., Legrand, M., McConnell, J.: 2012, *Geophys. Res. Lett.* **39**, L08503.
Yiou, F., Raisbeck, G.M., Baumgartner, S., Beer, J., Hammer, C., Johnsen, S., Jouzel, J., Kubik, P.W., Lestringuez, J., Stiévenard, M., Suter, M., Yiou, P.: 1997, *J. Geophys. Res.* **102**, 26783.
Zeller, E.J., Parker, B.C.: 1981, *Geophys. Res. Lett.* **8**, 895.